MONITORING OF CURE AND THERMAL SHRINKAGE IN INTERLAYER-TOUGHENED CFRP LAMINATES

K. Ogi[1], K. Mizukami[2], H. Matsutani[3] and N. Sato[4]

[1]Graduate School of Science and Engineering, Ehime University, 3, Bunkyo-cho, Matsuyama, Ehime 790-8577, Japan
Email: ogi.keiji.mu@ehime-u.ac.jp, Web Page: https://www.me.ehime-u.ac.jp
[2]Graduate School of Science and Engineering, Ehime University, 3, Bunkyo-cho, Matsuyama, Ehime 790-8577, Japan
Email: mizukami.koichi.tp@ehime-u.ac.jp, Web Page: https://www.me.ehime-u.ac.jp
[3]Composite Materials Research Laboratories, Toray Industries, Inc., 1515, Tsutsui, Masaki, Ehime 791-3193, Japan
Email: Hiroaki_Matsutani@nts.toray.co.jp, Web Page: http://www.toray.com
[4]Composite Materials Research Laboratories, Toray Industries, Inc., 1515, Tsutsui, Masaki, Ehime 791-3193, Japan
Email: Narumichi_Sato@nts.toray.co.jp, Web Page: http://www.toray.com

Keywords: cure shrinkage, thermal shrinkage, interlayer, monitoring, FBG sensor

Abstract
This paper presents in-process monitoring of cure and thermal shrinkage in unidirectional (UD) CF/Epoxy laminates with interlayers. The transverse strain during a cure-process was in-situ measured using an FBG sensor embedded in UD laminates with interlayers (IL) and without interlayers (NIL). From the strain during a hold (high-temperature) stage, the coefficient of cure shrinkage (CCS) in the transverse direction was estimated for both laminates. On the other hand, the coefficient of thermal expansion (CTE) in the transverse direction was calculated from the change in the strain during a cooling stage. The CTEs of both laminates were also measured by thermomechanical analysis for cured samples. The CCS of the IL laminate is lower than that of the NIL laminate while the transverse CTE of the IL laminate is higher than that of the NIL laminate. The CTE of both laminates decreases as the temperature decreases. This temperature dependence of CTE is more prominent in the thickness direction. The above difference of CCS and CTE in both laminates is approximately explained using micromechanical models. However, some discrepancy could be attributed to softening of thermoplastic particles and temperature dependent Young's modulus with large error in the interlayer.

1. Introduction

As application of carbon fiber reinforced thermosetting resin composite (CFRP) laminates have been extended to primary structure of civil aircraft, high-cycle fabrication has been increasingly required. Since the conventional autoclave method needs much cost and processing time, several out-of-autoclave (OoA) fabrication methods have been developed. In any fabrication methods, unexpected deformation such as spring-in must be minimized to assure the dimensional accuracy and structural integrity. It has been reported that a lot of factors such as viscoelastic properties, chemical (cure) shrinkage and thermal shrinkage affect the residual stress during and after a cure process.

Several mathematical models including viscoelastic ones have been proposed thus far to predict the process-induced deformation of thermosetting resin composites. For example, Johnston et al. [1] proposed the cure-hardening instantaneously linear elastic (CHILE) constitutive model where the elastic moduli of the resin change depending on temperature and DOC. In the path-dependent constitutive

(PDC) model [2], the relaxation moduli before and after vitrification are approximated to be ones in the rubbery and glassy states, respectively. Zobeiry et al. [3] then proposed the pseudo-viscoelastic (PVE) model where the modulus at a particular time or frequency can be regarded as the modulus in the CHILE model. In addition, Kravchenko et al. [4] employed a simple modulus development model using two storage moduli during hold and cooling stages. Minakuchi et al. [5] performed cure simulation based on the incremental linear elastic (ILE) model employing the internal strain measured with fiber Bragg grating (FBG) sensors.

The latest CFRP prepreg for aircraft such as T800S/3900-2B (Toray) includes interlayers with thermoplastic particles which enhance the interlaminar fracture toughness to suppress delamination. Although a lot of work has been performed in terms of fracture behavior of such CFRP, little attention has been paid to fabrication simulation considering internal strains except in several papers [6, 7]. According to the previous work, one of the difficulties in computational simulation is attributed to unknown material properties depending on temperature and degree of cure (DOC).

Hence, this paper presents in-process monitoring of cure and thermal shrinkage in unidirectional (UD) CF/Epoxy laminates with interlayers. The transverse strain during a cure-process was in-situ measured using FBG sensors embedded in UD laminates with interlayers (IL) and without interlayers (NIL). From the strain during a hold (high-temperature) stage, the coefficient of cure shrinkage (CCS) in the transverse direction was estimated for both laminates. On the other hand, the coefficient of thermal expansion (CTE) in the transverse direction was calculated from the change in the strain during a cooling stage. Moreover, the CTEs in the fiber, transverse and thickness directions of both laminates were measured by thermomechanical analysis (TMA) for cured samples. Finally, the CCS and CTE in both laminates were discussed using micromechanical models.

2. Experimental

2.1. In-process monitoring

The NIL laminates were fabricated using the prepreg consisting of carbon fiber (T800S) and epoxy resin (CFRP baes ply) while the IL laminates were made of the prepreg consisting of a CFRP base ply and an interlayer including thermoplastic particles. The thickness of the prepreg of the NIL and IL laminates is 180 and 200 μm, respectively. The material properties of the NIL laminates at room temperature are similar to those of T800S/3900-2B and appear in the literature [7]. Both prepregs were cut into 75 mm square sheets. The number of stacking plies n of the NIL and IL laminates is 24 and 20, respectively. An FBG sensor was embedded in the mid-plane so that the direction of the FBG sensor was normal to the fiber. The thermocouple was employed to measure the temperature of the laminate. A unidirectional laminate ($[0^{o}_{n}]$) set in a vacuum bag was fabricated using an autoclave. The laminate was heated up to 180 ^{o}C at a rate of 2 ^{o}C/min. After the laminate was kept at 180 ^{o}C for two hours, it was cooled down to room temperature at a rate of - 2 ^{o}C/min. The internal pressure of the autoclave was maintained at 0.2 MPa during the whole cure-process. The thickness of the cured NIL and IL laminates is 3.9 mm and 3.8 mm, respectively, and the final DOC after the cure-process is 0.90 [7].

Figure 1 depicts the experimental setup for in-process monitoring of the internal strain and temperature. The central wave length and gage length of the FBG sensor are 1550 nm and 1 mm, respectively. The wave length spectrum of the laser ray reflected from the FBG sensor was measured at a sampling rate of 0.5 sec using a spectrum analyzer built in an FBG interrogator (sm125, Micron Optics). The signals of the wave length spectrum and the temperature were collected in a personal computer to calculate the mechanical strain ε due to cure and thermal shrinkage using the following equation:

$$\varepsilon = C_{\mathrm{S}}\left(\Delta\lambda_{\mathrm{B}} - \frac{\Delta T}{C_{\mathrm{T}}}\right) \quad (1)$$

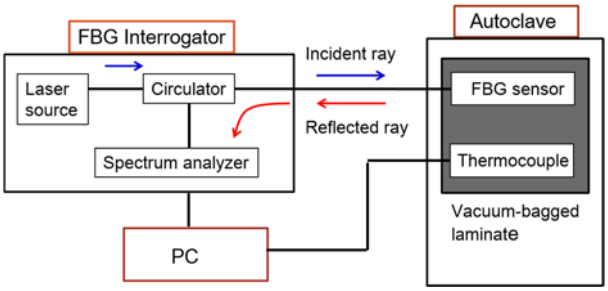

Figure 1. Data acquisition system for in-process monitoring of internal strain using an FBG sensor.

where $\Delta\lambda_B$ and ΔT respectively denote the wave length shift and the temperature change from the room temperature. C_S and C_T are the correction factors associated with strain and temperature, respectively, and the calibrated values of C_S and C_T are 826.1 με/nm and 88.34 °C /nm, respectively. Five or six specimens were employed for monitoring the strain. The CCSs and CTEs in the transverse direction of both laminates were calculated from the measured transverse strains in the hold and cooling stages, respectively.

2.2. TMA measurement

NIL and IL UD laminates [0^o_n] with DOC of 0.90 were prepared through the same cure-process as above. The cured thickness of the NIL and IL laminates is 5.4 mm and 5.8 mm, respectively. The laminates were cut into 5 mm square samples for TMA measurement. The sample was heated up to 200 °C at a heating rate of 2 °C/min in a sample tube of TMA. The probe load applied to the sample was selected to be 50 mN. The CTEs in the fiber, transverse and thickness directions were measured using two samples for each direction.

3. Micromechanical model

3.1 Elastic constants

In order to predict the CCSs and CTEs of both laminates, the micromechanical model is used. In this section, elastic constants are described. First, we assume that the Poisson's ratio of the epoxy resin ν_m is constant. This assumption is reasonable when the resin becomes glassy after gelation [8]. The shear modulus of the resin G_m is then proportional to E_m. Second, the elastic constants of fiber are assumed to be constant during a cure-process. Since the IL laminate can be regarded as a transversely isotropic body, the elastic constants of the IL laminate are given by

$$E_{11} = E_{11f}V_f + E_m(1-V_f) + \frac{4(\nu_m - \nu_{12f})^2 k_f k_m G_m (1-V_f)V_f}{(k_f + G_m)k_m + (k_f - k_m)G_m V_f} \quad (1)$$

$$E_{22} = E_{33} = \frac{1}{(1/4k_T) + (1/4G_{23}) + (\nu_{12}^2/E_{11})} \quad (2)$$

$$G_{12} = G_{13} = G_m\left[\frac{(G_{12f} + G_m) + (G_{12f} - G_m)V_f}{(G_{12f} + G_m) - (G_{12f} - G_m)V_f}\right] \quad (3)$$

$$\nu_{12} = \nu_{13} = \nu_{12f}V_f + \nu_m(1-V_f) + \frac{(\nu_m - \nu_{12f})(k_m - k_f)G_m(1-V_f)V_f}{(k_f + G_m)k_m + (k_f - k_m)G_m V_f} \quad (4)$$

where E, G, k and ν are respectively referred to as the Young's modulus, shear modulus, bulk modulus and Poisson's ratio, the subscripts 1, 2 and 3 respectively denote the properties of the fiber, transverse and thickness directions, the subscripts f and m represent the properties of fiber and resin, respectively,

and V_f is the fiber volume fraction. The expressions for G_{23}, ν_{23}, G_m,$G_{23\mathrm{f}}$, k_T, k_m and k_f are given elsewhere [4, 5, 7]. From the above equations, all the elastic constants are expressed as functions of E_m.

The prepreg of the IL laminate consists of a CFRP base ply (thickness t_c) and an interlayer (thickness t_i). When it is assumed that the interlayer on the transversely-isotropic base ply is isotropic, the IL laminate can be treated as a homogeneous orthotropic body. Consequently, the in-plane elastic constants of the IL laminate are approximated by the following simple rule of mixture:

$$\bar{E}_{11} = E_\mathrm{i}V_\mathrm{i} + E_{11}(1 - V_\mathrm{i}) \tag{5}$$

$$\bar{E}_{22} = E_\mathrm{i}V_\mathrm{i} + E_{22}(1 - V_\mathrm{i}) \tag{6}$$

$$\bar{\nu}_{12} = \nu_\mathrm{i}V_\mathrm{i} + \nu_{12}(1 - V_\mathrm{i}) \tag{7}$$

$$\bar{G}_{12} = G_\mathrm{i}V_\mathrm{i} + G_{12}(1 - V_\mathrm{i}) \tag{8}$$

with

$$V_\mathrm{i} = \frac{t_\mathrm{i}}{t_\mathrm{i} + t_\mathrm{c}} \tag{9}$$

$$E_\mathrm{i} = E_\mathrm{m}V_\mathrm{e} + E_\mathrm{p}(1 - V_\mathrm{e}) \tag{10}$$

where the subscripts i and p respectively stand for the properties of the interlayer and thermoplastic particles, V_e represents the volume fraction of epoxy resin in the interlayer, and a bar over the variable denotes the properties of the IL laminate.

3.2. CTE

It is well known that β_m depends on temperature T and DOC α. Here, the following simple expression is proposed for epoxy resin during cure:

$$\beta_\mathrm{m} = \begin{cases} b_{\mathrm{m}1} & (\alpha \le \alpha_\mathrm{gel}) \\ b_{\mathrm{m}2}(T) & (\alpha \ge \alpha_\mathrm{gel}) \end{cases} \tag{11}$$

where $b_{\mathrm{m}1}$ is a material constant and $b_{\mathrm{m}2}(T)$ is a function of temperature. The expression for the CTE of the interlayer is proposed as follows:

$$\beta_\mathrm{i} = \frac{\beta_\mathrm{m}E_\mathrm{m}V_\mathrm{e} + \beta_\mathrm{p}E_\mathrm{p}(1 - V_\mathrm{e})}{E_\mathrm{i}} \tag{12}$$

where β_p and E_p respectively denote the CTE and Young's modulus of thermoplastic resin particles. The CTEs of the NIL laminate, β_j $(j = 1, 2, 3)$, are given by the micromechanical model [9] as

$$\beta_1 = \frac{\beta_{1\mathrm{f}}E_{11\mathrm{f}}V_\mathrm{f} + \beta_\mathrm{m}E_\mathrm{m}(1 - V_\mathrm{f})}{E_{11}} \tag{13}$$

$$\beta_2 = \beta_3 = (\beta_{2\mathrm{f}} + \nu_{12\mathrm{f}}\beta_{1\mathrm{f}})V_\mathrm{f} + (1 + \nu_\mathrm{m})\beta_\mathrm{m}(1 - V_\mathrm{f}) - \nu_{12}\beta_1 \tag{14}$$

Finally, the CTE of the IL laminate, $\bar{\beta}_j$ $(j = 1, 2, 3)$, are analogous to Eqs. (13) and (14):

$$\bar{\beta}_1 = \frac{\beta_\mathrm{i}E_\mathrm{i}V_\mathrm{i} + \beta_1E_{11}(1 - V_\mathrm{i})}{\bar{E}_{11}} \tag{15}$$

$$\bar{\beta}_2 = \frac{\beta_\mathrm{i} E_\mathrm{i} V_\mathrm{i} + \beta_2 E_{22}(1 - V_\mathrm{i})}{\bar{E}_{22}} \tag{16}$$

$$\bar{\beta}_3 = (\beta_2 + \nu_{12}\beta_1)(1 - V_\mathrm{i}) + (1 + \nu_\mathrm{i})\beta_\mathrm{i} V_\mathrm{i} - \bar{\nu}_{12}\bar{\beta}_1. \tag{17}$$

It should be noted that CTE of the thickness direction is different from that of the transverse direction.

3.3. CCS

The cure shrinkage strain rate of the NIL laminate is expressed as

$$\dot{\varepsilon}_j = -\lambda_j \dot{\alpha} \quad (j = 1, 2, 3) \tag{18}$$

where λ_j denotes the CCS of the NIL laminate in the *j*-direction. When the volumetric shrinkage strain of epoxy resin λ_m is provided, λ_j $(j = 1, 2, 3)$ are expressed as

$$\lambda_1 = \frac{(\lambda_\mathrm{m}/3) E_\mathrm{m}(1 - V_\mathrm{f})}{E_{11\mathrm{f}} V_f + E_\mathrm{m}(1 - V_\mathrm{f})} \tag{19}$$

$$\lambda_2 = \lambda_3 = (\lambda_\mathrm{m}/3)(1 + \nu_m)\big(1 - V_f\big) - \nu_{12}\lambda_1 \tag{20}$$

in which the expressions of CTE (Eqs. (13) and (14)) are employed by replacing $\beta_{j\mathrm{f}}$ and β_m with 0 and $\lambda_\mathrm{m}/3$, respectively. The CCSs of the IL laminate $\bar{\lambda}_j$ $(j = 1, 2, 3)$ are then given by

$$\bar{\lambda}_1 = \frac{(\lambda_\mathrm{i}/3) E_\mathrm{i} V_\mathrm{i} + \lambda_1 E_{11}(1 - V_\mathrm{i})}{\bar{E}_{11}} \tag{21}$$

$$\bar{\lambda}_2 = \frac{(\lambda_\mathrm{i}/3) E_\mathrm{i} V_\mathrm{i} + \lambda_2 E_{22}(1 - V_\mathrm{i})}{\bar{E}_{22}} \tag{22}$$

$$\bar{\lambda}_3 = (\lambda_2 + \nu_{12}\lambda_1)(1 - V_\mathrm{i}) + (1 + \nu_\mathrm{i})(\lambda_\mathrm{i}/3) V_\mathrm{i} - \bar{\nu}_{12}\bar{\lambda}_1 \tag{23}$$

in which the expressions of CTE (Eqs. (15) to (17)) are employed by replacing β_j and β_i with λ_j and $\lambda_\mathrm{i}/3$, respectively, and λ_i denotes the maximum volumetric shrinkage strain due to cure in the interlayer.

4. Results and discussion

Figure 2 shows the change in the temperature and the transverse strains in the NIL and IL laminates in a cure-process. After the gelation point ($\alpha_\mathrm{gel} = 0.65$), the strain decreases with time during the hold stage. In the subsequent cooling stage, the strain continues to decrease with a temperature decrease. The average cure and thermal shrinkage strains in the NIL and IL laminates are summarized in Table 1. The cure shrinkage of the IL laminate is smaller than that of the NIL laminate while the thermal shrinkage strain of the IL laminate is greater than that of the NIL laminate.

Figure 3 (a) demonstrates the CTE of the NIL and IL laminates calculated from the strain in the cooling stage (Fig. 2). The CTE of both laminates increases with increasing temperature. The increase is remarkable when the temperature exceeds approximately 80 °C. The CTE of the IL laminate is larger than that of the NIL laminate at temperature below 140 °C. This temperature dependence of CTE is expressed by the following empirical equation:

$$\left.\begin{matrix}\beta_2(T)\\ \bar{\beta}_2(T)\end{matrix}\right\} = \begin{cases} a(T - 50)^2 + b \\ \bar{a}(T - 50)^2 + \bar{b} \end{cases} \quad \big(T \geq 50\ ^\circ\mathrm{C},\ \alpha \geq \alpha_\mathrm{gel}\big) \tag{24}$$

where a, b, $\bar{a}$ and $\bar{b}$ are material constants. The values of a, b, $\bar{a}$, $\bar{b}$, CCS and CTE of both laminates are listed in Table 2 where the CCS at DOC lower than α_gel is assumed to be zero for simplicity. Combining eqs. (11), (14) and (24) leads to

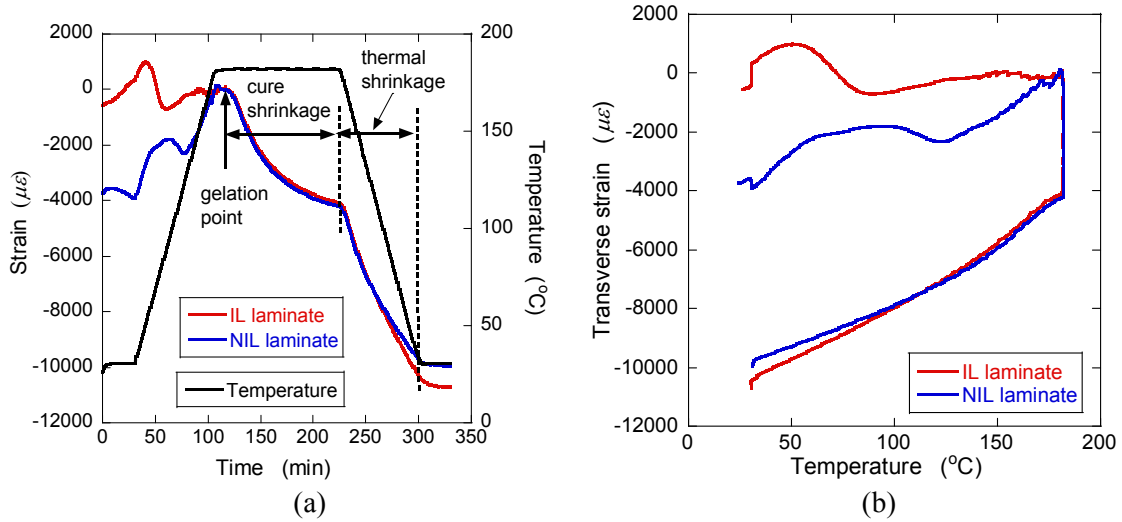

Figure 2. Change in the temperature and the transverse strains in the NIL and IL laminates in a cure-process ((a): strain and temperature vs. time, (b): strain vs. temperature).

Table 1. Average cure and thermal shrinkage strains in the NIL and IL laminates.

Laminate	Cure shrinkage strain ($\mu\varepsilon$)	Thermal shrinkage strain ($\mu\varepsilon$)
NIL	4200	5800
IL	4000	6100

$$b_{\mathrm{m2}}(T) = \frac{a}{(1+\nu_{\mathrm{m}})(1-V_{\mathrm{f}})}(T-50)^2 + \frac{b-(\beta_{2\mathrm{f}}+\nu_{12\mathrm{f}}\beta_{1\mathrm{f}})V_{\mathrm{f}}}{(1+\nu_{\mathrm{m}})(1-V_{\mathrm{f}})} \quad (\alpha \geq \alpha_{\mathrm{gel}}) \tag{25}$$

Temperature dependence of CTE of the NIL laminate, $\beta_2(T)$, IL laminate, $\bar{\beta}_2(T)$, and epoxy resin, $b_{\mathrm{m2}}(T)$, is compared in Fig. 3 (a). It is proved that the increase in CTE of both laminates is mainly attributed to the temperature dependence of CTE of the epoxy resin.

On the other hand, the measured Young's modulus of the epoxy resin with $\alpha = 0.90$ is expressed as [7]:

$$E_{\mathrm{m}}(T) = \begin{cases} E^{\mathrm{f}}_{m0,\mathrm{K}}\{1+p_{\mathrm{L}}(T_{\mathrm{K}}-T)\} & (T<T_{\mathrm{K}}) \\ E^{\mathrm{f}}_{m0,\mathrm{K}}\{1+p_{\mathrm{H}}(T_{\mathrm{K}}-T)\} & (T>T_{\mathrm{K}}) \end{cases} \tag{26}$$

where $E^{\mathrm{f}}_{m0,\mathrm{K}} = 2.42$ GPa, $p_{\mathrm{L}} = 0.00385$ (°C^{-1}), $p_{\mathrm{H}} = 0.0115$ (°C^{-1}) and $T_{\mathrm{K}} = 140$ °C. It could be possible to determine $E_{\mathrm{i}}(T)$ using measured $E_{22}(T)$ and $\bar{E}_{22}(T)$ according to Eq. (6). However, the difference between E_{22} and $\bar{E}_{22}$ during the cure-cycle was not always large enough to precisely estimate $E_{\mathrm{i}}(T)$. Therefore, it is assumed that $E_{\mathrm{i}}(T)$ changes in proportion to E_m. Figure 3 (b) depicts

Table 2. Parameters associated with cure and thermal shrinkage in the NIL and IL laminates.

Laminate	a or $\bar{a}$ (°C^{-3})	b or $\bar{b}$ (°C^{-1})	Transverse CCS, λ_2 or $\bar{\lambda}_2$ (Upper: $0 \leqq \alpha \leqq \alpha_{\mathrm{gel}}$) (Lower: $\alpha_{\mathrm{gel}} \leqq \alpha \leqq 0.90$)	Transverse CTE, β_2 or $\bar{\beta}_2$ ($50 \leqq T \leqq 80$ °C) (x 10^{-6} °C^{-1})
NIL	0.00254	26.7	0 0.0168	27.5
IL	0.00189	32.5	0 0.0160	33.1

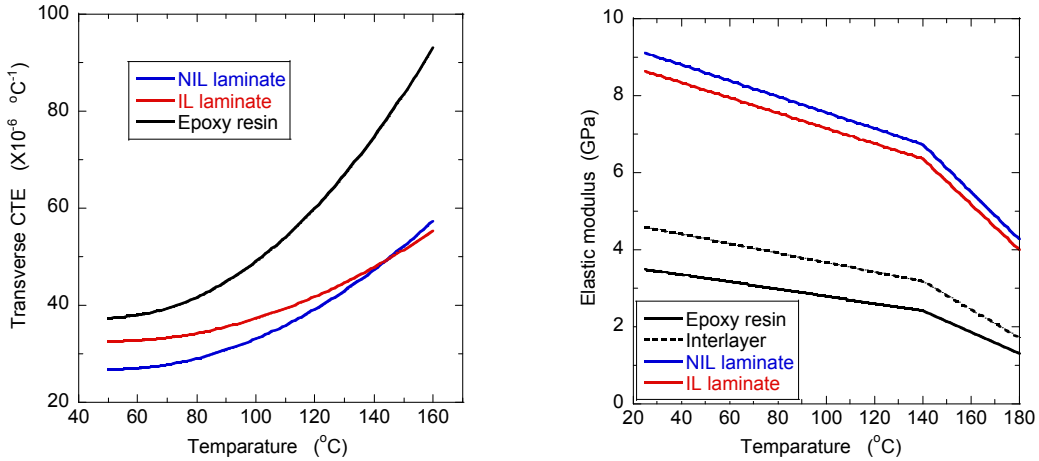

Figure 3. Change in (a) the CTE of the NIL and IL laminates and the epoxy resin and (b) the elastic modulus of the epoxy resin, interlayer and the NIL and IL laminates in the cooling stage.

the change in the Young's modulus of the epoxy resin and the interlayer and the transverse modulus of the NIL and IL laminates calculated using eqs. (2), (6) and (26). It is found that the moduli increase bilinearly with cooling. Using eq. (22) and the moduli in Fig. 3 (b), the predicted λ_i is -0.00282. This value is evidently incorrect. This is partly because softening of the thermoplastic particles in the interlayer prevent the FBG sensor from fully capturing the cure shrinkage strain. Another reason is the small difference between the measured $E_{22}(T)$ and $\bar{E}_{22}(T)$.

Figure 4 (a) shows the CTE of the NIL and IL laminates in the fiber, transverse and thickness directions measured by TMA. The CTE in the fiber direction is approximately zero independent of temperature while the CTEs in the transverse and thickness directions exhibit temperature dependence as shown in Fig. 3 (a). The CTEs in the transverse direction measured by TMA are lower than those measured by FBG sensors, especially at high temperatures. This discrepancy is attributed to the increase in higher DOC of the TMA samples which undergo after-cure. In addition, the CTEs measured by FBG sensors

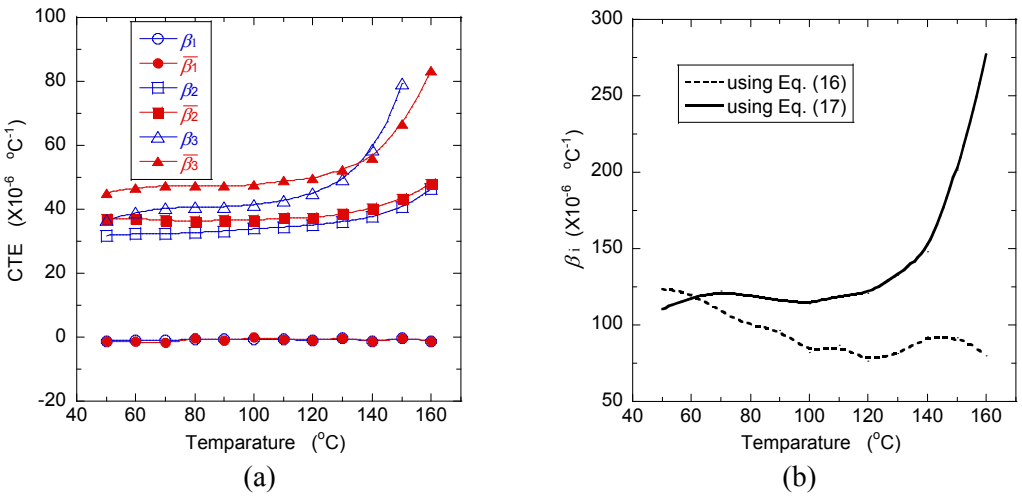

Figure 4. (a) The CTE of the NIL and IL laminates in the three directions measured by TMA and (b) the CTE of the interlayer estimated using eqs. (16) and (17).

and TMA are the ones in the cooling and heating, respectively. The CTE in the thickness direction is higher than that in the transverse direction. Figure 4 (b) plots the CTE of the interlayer estimated from this result and eqs. (16) and (17). The two values are comparable only at low temperatures. Equation (17) can provide better prediction because it does not employ the temperature dependent elastic moduli $E_{22}(T)$ and $\bar{E}_{22}(T)$ that are not always accurately measured.

5. Conclusions

This paper presents cure and thermal shrinkage strains in UD NIL and IL laminates using embedded FBG sensors and TMA. It is found that the CCS of the IL laminate is lower than that of the NIL laminate while the transverse CTE of the IL laminate is higher than that of the NIL laminate. The CTE of both laminates decreases as the temperature decreases in the cooling stage. This temperature dependence of CTE is more prominent in the thickness direction. The above difference of CCS and CTE in both laminates is approximately explained using micromechanical models. However, some discrepancy must be attributed to softening of thermoplastic particles in the interlayer and inaccurate temperature dependent elastic moduli during the cure process.

Acknowledgments

This research was supported by Cross-ministerial Strategic Innovation Promotion Program (SIP) of Japan Science and Technology Agency (JST).

References

[1] A. Johnston, R. Vaziri and A. Poursartip. A plane strain model for process-induced deformation of laminated composite structures. *J. Compos. Maters.*, 35:1435-1469, 2001.

[2] J. M. Svanberg and J. A. Holmberg. Prediction of shape distortions Part I. FE-implementation of a path dependent constitutive model. *Composites A*, 35: 711-721, 2004.

[3] N. Zobeiry, R. Vaziri and A. Poursartip. Computationally efficient pseudo-viscoelastic models for evaluation of residual stresses in thermoset polymer composites during cure. *Composites A*, 41: 247-56, 2010.

[4] O. G. Kravchenko, S. G. Kravchenko and R. B. Pipes. Chemical and thermal shrinkage in thermosetting prepreg. *Composites A*, 80: 72-81, 2016.

[5] S. Minakuchi, S. Niwa, K. Takagaki and N. Takeda. Composite cure simulation scheme fully integrating internal strain measurement. *Composites A*, 84: 53-63, 2016.

[6] S. Niwa S, K. Takagaki, S. Minakuchi and N. Takeda. Cure shrinkage monitoring and process analysis of CFRP laminates with interlaminar-resin layers. *J. Japan Soc. Compos. Maters.*, 41:168-175, 2015.

[7] K. Ogi, M. Tsutsumi, K. Mizukami, H. Matsutani and N. Sato. Numerical simulation of process-induced deformation of carbon/epoxy composite laminates with interlayers. *Proceedings of the 15th Japan International SAMPE Symposium and Exhibition*, Tokyo, Japan, November 27-29 2017.

[8] N. Ersoy, T. Garstka, K. Potter, M. R. Wisnom, D. Porter, M. Clegg and G. Stringer. Development of the properties of a carbon fibre reinforced thermosetting composite through cure. *Composites A*, 41: 401-409, 2010.

[9] R. A. Schapery. Thermal expansion coefficients of composite materials based on energy principles. *J. Compos. Maters.*, 2: 80-404, 1968.